1 **Chloroplasts Require Glutathione Reductase to Balance Reactive Oxygen**

2 **Species and Maintain Efficient Photosynthesis**

3

4 Stefanie J. Müller-Schüssele[1*], Ren Wang[2], Desirée D. Gütle[3], Jill Romer[4], Marta

5 Rodriguez-Franco[5], Martin Scholz[2], Volker M. Lüth[3], Stanislav Kopriva[6], Peter

6 Dörmann[4], Markus Schwarzländer[2], Ralf Reski[3,7], Michael Hippler[2], Andreas J.

7 Meyer[1*]

8

9 [1] Institute of Crop Science and Resource Conservation (INRES), University of Bonn, Friedrich-Ebert-

10 Allee 144, 53113 Bonn, Germany

11 [2] Institute of Plant Biology and Biotechnology, University of Münster, Schlossplatz 8, 48143 Münster,

12 Germany

13 [3] Plant Biotechnology, Faculty of Biology, University of Freiburg, Schänzlestr.1, 79104 Freiburg,

14 Germany

15 [4] Institute of Molecular Physiology and Biotechnology of Plants, University of Bonn, 53115 Bonn,

16 Germany

17 [5] Faculty of Biology, Cell Biology, University of Freiburg, Schänzlestr. 1, 79104 Freiburg, Germany

18 [6] Botanical Institute, Cluster of Excellence on Plant Sciences (CEPLAS), University of Cologne,

19 Cologne, Germany

20 [7] Signalling Research Centres BIOSS and CIBSS, University of Freiburg, Schänzlestr.18, 79104

21 Freiburg, Germany

22

23

24 * Correspondence

25 Stefanie Müller-Schüssele, Friedrich-Ebert-Allee 144, 53113 Bonn, Germany

26 phone number: +49 228 73 54266

27 e-mail: stefanie.mueller@uni-bonn.de

28

29 Andreas Meyer, Friedrich-Ebert-Allee 144, 53113 Bonn, Germany

30 phone number: +49 228 73 60353

31 e-mail: andreas.meyer@uni-bonn.de

32

33

1

Summary

(1) Thiol-based redox-regulation is vital to coordinate chloroplast functions depending on illumination. Yet, how the redox-cascades of the thioredoxin and glutathione redox machineries integrate metabolic regulation and reactive oxygen species (ROS) detoxification remains largely unresolved. We investigate if maintaining a highly reducing stromal glutathione redox potential (E_{GSH}) via glutathione reductase (GR) is necessary for functional photosynthesis and plant growth.

(2) Since absence of the plastid/mitochondrial GR is embryo-lethal in *Arabidopsis thaliana*, we used the model moss *Physcomitrella patens* to create knock-out lines. We dissect the role of GR in chloroplasts by *in vivo* monitoring stromal E_{GSH} dynamics, and reveal changes in protein abundances by metabolic labelling.

(3) Whereas stromal E_{GSH} is highly reducing in wildtype and clearly responsive to light, the absence of GR leads to a partial oxidation, which is not rescued by light. Photosynthetic performance and plant growth are decreased with increasing light intensities, while ascorbate and zeaxanthin levels are elevated. An adjustment of chloroplast proteostasis is pinpointed by the induction of plastid protein repair and degradation machineries.

(4) Our results indicate that the plastid thioredoxin and glutathione redox systems operate largely independently. They reveal a critical role of GR in maintaining efficient photosynthesis.

Keywords: Chloroplast**,** glutathione redox potential, light stress, *Physcomitrella patens,* redox-sensitive GFP, ROS

Introduction

In photosynthetic eukaryotes, changes in environmental conditions, such as light intensity or temperature, provoke changes in electron flow both in the chloroplasts and in the mitochondria. Several mechanisms serve to rapidly modulate or redirect electron flow to minimise over-reduction of the two electron transport chains (ETCs), which can otherwise give rise to excessive formation of reactive oxygen species (ROS) (Schwarzländer & Finkemeier, 2013; Schöttler & Toth, 2014). Moreover, ROS serve as important signalling molecules in stress acclimation (Suzuki *et al.*, 2012; Dietz *et al.*, 2016). This implies that the rates of ROS generation and scavenging must be precisely balanced in these organelles. The maintenance of cellular redox

2

68 pools for metabolism, antioxidant defence, and thiol-based redox switching requires
69 the constant influx of electrons via light- and NADPH-powered redox cascades,
70 involving the oxidation and reduction of cysteines in thioredoxins (Trx) and
71 glutathione (Meyer *et al.*, 2012; Yoshida & Hisabori, 2016; Geigenberger *et al.*, 2017;
72 Gütle *et al.*, 2017).

73 Reduced glutathione (GSH) is present in cells at low millimolar concentrations (Meyer
74 *et al.*, 2001). Glutathione functions include ascorbate regeneration via the ascorbate-
75 glutathione-cycle and detoxification of potentially toxic organic electrophils and heavy
76 metals, as well as acting as a cofactor of monothiol glutaredoxins (Grx) for
77 coordination of iron-sulfur clusters (Foyer & Noctor, 2011; Moseler *et al.*, 2015). In
78 addition, glutathione is also used as a substrate of dithiol Grx-catalysed protein
79 (de)glutathionylation (Meyer *et al.*, 2012; Zaffagnini *et al.*, 2019). For the latter
80 functions it is essential that glutathione can reversibly switch between its reduced
81 form GSH and the oxidised form glutathione disulfide (GSSG) which involves the
82 transfer of 2 electrons. The glutathione redox potential (E_{GSH}) is dependent on the
83 GSH concentration, as well as on the balance between GSH and GSSG. The E_{GSH}
84 can vary drastically between subcellular compartments (Meyer, 2008; Kojer *et al.*,
85 2012). In unstressed plant cells, the E_{GSH} of cytosol, peroxisomes, mitochondrial
86 matrix and plastid stroma is highly reducing between -310 to -360 mV (Meyer *et al.*,
87 2007; Schwarzländer *et al.*, 2008). In these compartments, GSSG is efficiently
88 regenerated to GSH by the action of glutathione reductase (GR) using NADPH as
89 electron donor. In the cytosol and the mitochondria of *Arabidopsis thaliana* the loss of
90 GR is partially compensated for by the presence of the NADPH-dependent Trx
91 reductases A and B (NTRA,B) (Marty *et al.*, 2009). Nevertheless, decreased GR
92 activity of the plastid/mitochondria-targeted isoform leads to reduced root growth in
93 seedlings (Yu *et al.*, 2013). However, a complete loss of GR in plastids causes
94 embryo-lethality (Marty *et al.*, 2009; L. Marty & A.J. Meyer, unpublished).

95 Since this limits the usability of Arabidopsis as a model for GR function in green
96 plastids, the significance of GR in stromal E_{GSH} maintenance, for photosynthesis and
97 other plastid functions has remained unclear. Further, it is unknown to what extent
98 the Trx system can serve as a back-up for the glutathione redox system in plastids.

99 Here, we investigate the effects of the complete loss of plastid/mitochondria-localized
100 GR in photosynthetic cells, utilising the moss *Physcomitrella patens* as a model
101 (Reski, 2018). We assess growth and photosynthetic parameters, monitor the

3

102 dynamics of plastid E_{GSH} by redox-sensitive GFP (roGFP)-based *in vivo* imaging and

103 compare protein abundances between wildtype (WT) and GR mutants in response to

104 a shift from low light to high light by quantitative proteomics.

105

Material and Methods

Plant materials and growth conditions

108 *Physcomitrella patens* (Hedw.) B.S. ecotype 'Gransden 2004' (International Moss

109 Stock Centre (IMSC, http://www.moss-stock-center.org), accession number 40001)

110 was grown axenically in agitated liquid Knop medium (250 mg l^{-1} KH_2PO_4, 250 mg l^{-1}

111 KCl, 250 mg l^{-1} $MgSO_4$ x $7H_2O$,1 g l^{-1} $Ca(NO_3)_2$ x $4H_2O$ and 12.5 mg l $FeSO_4$ x $7H_2O$,

112 pH 5.8) (Reski & Abel, 1985) with micro-elements (ME) (H_3BO_3, $MnSO_4$, $ZnSO_4$, KI,

113 Na_2MoO_4 x $2H_2O$, $CuSO_4$, $Co(NO_3)_2$) (Egener *et al.*, 2002) in a growth cabinet under

114 long day conditions (16 h:8 h, light:dark, 22°C) at 100 µmol photons m^{-2} s^{-1}. For

115 phenotypic and pigment analyses, *P. patens* was grown on KNOP ME agar plates

116 (12 g l^{-1} purified agar, Oxoid) at the indicated light intensity.

117 For measurements of photosynthetic parameters and preparation of proteins

118 samples for MS/MS, *P. patens* protonema tissue was propagated under axenic

119 conditions either on 9 cm or 4.5 cm Petri dishes overlaid with a cellophane disk on

120 solidified $PpNO_3$ medium（0.8 % (w/v) agar), or in glass flasks with $PpNO_3$ medium

121 (Gerotto *et al.*, 2016) in a growth chamber under low light conditions (LL, 15 µmol

122 photons m^{-2} s^{-1}) at 25°C with a 16 h:8 h light:dark photoperiod. For control and high

123 light assays, 10-day-old protonema plates were moved from LL to 50 µmol photons

124 m^{-2} s^{-1} (CL) and 450 µmol photons m^{-2} s^{-1} (HL) respectively, maintaining temperature

125 and photocycle.

126

Generation of PpGR1 knock-out lines

128 A knock-out construct for Pp1s13_127V6.1 was designed by amplifying homologous

129 regions from genomic DNA with primer pairs PpGR1ko_5PHR_F/

130 PpGR1ko_5PHR_R and PpGR1ko_3PHR_F/ PpGR1ko_3PHR_R (Table S1),

131 introducing BspQ1 restriction sites to the homologous ends. DNA fragments

132 containing homologous regions were joined with an expression cassette (Nopalin

133 synthase promoter and terminator) for hygromycin phosphotransferase (hpt) via

134 triple-template PCR. This construct eliminates a large part of the Pp1s13_127V6.1

135 coding sequence including the active site (Fig. S1a). The knock-out construct was

4

136   subsequently ligated into the pJET1.2 (Thermo Scientific) vector, digested with

137   BspQ1 and introduced via PEG-mediated protoplast transformation (Hohe *et al.*,

138   2004) into a newly generated line expressing *TKTP-Grx1-roGFP2* (Schwarzländer *et*

139   *al.*, 2008; Speiser *et al.*, 2018) stably integrated at the PTA2 locus under the control

140   of the *PpActin5* promoter (Kubo *et al.,* 2013; Mueller & Reski, 2015). In regenerated

141   plants that survived hygromycin selection, integration of the construct into the target

142   locus was verified using primer pairs spanning the 5' integration site (5P_F and

143   H3b_R, Fig. S1b) and the 3' integration site (NosT_F and 3P_R) (Table S1). Absence

144   of *PpGR1* transcript for independent knock-out lines was confirmed using the primer

145   pair PpGR1_RT_F and PpGR1_RT_R in a reverse transcription PCR (Fig. S1c,

146   Table S1). Moss lines are available from the IMSC under the accession numbers:

147   TKTP-Grx1-roGFP2#40 IMSC 40836, Pp*gr1*#48 IMSC 40834, Pp*gr1*#88 IMSC

148   40835.

149

150   **Microscopy**

151   Microscopy was carried out using a Zeiss LSM780 (attached to an Axio Observer.Z1)

152   using a 25x (Plan-Apochromat 25x/0.8 Imm Korr NA0.8) or 40x (C-Apochromat

153   40×/1.2W Korr NA1.2) objective. Bright-field images were taken with an AxioCam

154   MRc. Confocal laser scanning microscopy of roGFP2 redox state was achieved by

155   consecutively exciting the roGFP2 with a 405 nm diode laser (at 2 % power output)

156   and a 488 nm Argon laser (at 1 % power output) in line switching mode, using

157   constant detector gain and emission from 508 to 535 nm. Autofluorescence was

158   recorded after excitation at 405 nm and emission from 430 to 470 nm. Chlorophyll

159   autofluorescence was monitored after 488 nm excitation at an emission of 680 to

160   735 nm. Image intensities and 405/488 nm ratios were calculated per pixel using a

161   custom MATLAB-based software using background subtraction and

162   autofluorescence correction (Fricker, 2016).

163

164   **Transmission electron microscopy**

165   Transmission electron microscopy (TEM) was performed as described in Schuessele

166   *et al.* (2016).

167

168

169

5

NBT staining

Gametophores were stained in a 0.1 mg/ml nitro blue tetrazolium (NBT, Duchefa) solution in 75 mM potassium phosphate buffer (pH 7.0) for 1.5 h in the dark or in the light (120 µmol photons $m^{-2}s^{-1}$). Chlorophyll was subsequently removed by incubation in 80 % ethanol at 70°C (Lee *et al.*, 2002).

Ascorbate assay

Total and reduced ascorbate in *P. patens* samples was quantified according to Gillespie & Ainsworth (2007) with the modification that 2-2'-bipyridyl was dissolved in 95 % ethanol. Five to 100 mg material was flash frozen in liquid nitrogen, homogenised in a bead mill (TissueLyser II, Qiagen, 30 Hz for 2x 1.5 min) and processed immediately.

Pigment and glutathione analysis by HPLC

Photosynthetic pigments were quantified by high-performance liquid chromatography (HPLC) according to Thayer & Björkman (1990), see also Supplemental Information. Glutathione was extracted from c. 30 mg protonema tissue (grown in c. 100 µmol photons $m^{-2}s^{-1}$) in 10-fold volume of 0.1 M HCl. After centrifugation for 10 min at 4°C, 25 µL of the supernatant were neutralised with 25 µL 0.1 M NaOH and thiols reduced with 1 µL 0.1 M dithiothreitol for 15 min at 37°C in darkness. Ten µL 1 M Tris/HCl pH 8.0, 35 µL water were added and the GSH was derivatised using 5 µL of 0.1 M monobromobimane (Thiolyte® MB, Calbiochem) in darkness for 15 min at 37°C. The reaction was stopped by adding 100 µL 9 % acetic acid and centrifugation at 4°C for 15 minutes. The bimane derivates were separated via HPLC (Spherisorb™ ODS2, 250 x 4.6 mm, 5 µm, Waters, Eschborn, Germany) using a linear gradient from 4 to 20 % of buffer A (90 % methanol (v/v), 0.25 % acetic acid (v/v), pH 3.9) in buffer B (10% methanol (v/v), 0.25 % acetic acid (v/v), pH 3.9) and detected fluorometrically with excitation at 390 nm and emission at 480 nm.

Metabolic labelling and MS/MS analysis

For isotopic labelling of *P. patens*, $Ca(NO_3)_2$ x $4H_2O$ in solid and liquid PpNO₃ media was replaced by $Ca(^{15}NO_3)_2$ x $4H_2O$ (Cambridge Isotope Laboratories, England). To obtain fully labelled protonema tissue the protonema cultures were weekly sub-cultivated on fresh ^{15}N labelled solid PpNO₃ media for at least 4 months. To quantify

6

204 differences in protein abundance between WT and *Δgr1* background, labelled and
205 unlabelled protonema of cpGrx1roGFP2 #40 and *Δgr1* #48 were shifted from LL to
206 HL for 1 h, including one label swap for each light intensity.

207 For protein extraction, c. 500 mg of *P. patens* protonema tissue was harvested and
208 the surface water removed. The samples were frozen in liquid nitrogen and 3x
209 homogenised using a MM300 mill (Retsch) for 30 s with a frequency of 30 s^{-1}.
210 Subsequently, 200-300 µl of protein extraction buffer (25 mM Trizma base, 1 % (w/v)
211 SDS, 5 mM EDTA, 0.5 mM PMSF, 0.5 mM Benzamidine) were added, centrifuged at
212 2000 x g for 2 min and protein concentration determined in the supernatant by
213 bicinchoninic acid assay. Equal protein amounts from ^{14}N and ^{15}N-labelled samples
214 were mixed and further processed in a filter-aided sample preparation protocol for
215 MS-based analysis according to Wiśniewski *et al.* (2009). All LC-MS/MS analyses
216 were carried out on a system composed of an Ultimate 3000 RSLCnano UPLC
217 coupled via a nanospray interface to a Q Exactive Plus mass spectrometer (Thermo
218 Fisher Scientific).

219

Shotgun Quantification

221 Peptides were pre-concentrated and desalted for 3 min on a trap column (Acclaim
222 PepMap 100, 300 µM x 5 mm, 5 µm particle size, 100 Å pore size, Thermo Fisher
223 Scientific) using 2 % (v/v) acetonitrile/0.05 % (v/v) trifluoroacetic acid in ultrapure
224 water at a flow rate of 10 µl/min. Gradient separation of peptides was performed on a
225 reversed phase column (C18, Acclaim Pepmap, 75 µm x 50 cm, 2 µm particle size,
226 100 Å pore size, Thermo Fisher Scientific) at a flow rate of 300 nl/min using the
227 eluents 0.1 % (v/v) formic acid in ultrapure water (A) and 80 % (v/v) acetonitrile/0.1 %
228 (v/v) formic acid in ultrapure water (B). The following gradient was applied: 2.5-18 %
229 B (v/v) over 105 min, 18-32 % B (v/v) over 55 min, 32-99 % B (v/v) over 5 min, 99 %
230 B (v/v) for 20 min.

231 MS full scans (MS1, *m/z* 300-1600) were acquired in positive ion mode at a
232 resolution of 70,000 (FWHM, at m/z 200) with internal lock mass calibration on *m/z*
233 445.120025. For MS2 the 12 most intense ions were fragmented by higher-energy c-
234 trap dissociation (HCD) at 27 % normalized collision energy (isolation window size:
235 1.5 m/z). Resolution for MS2 scans: 17,500 (FWHM, at *m/z* 200), target values for
236 automatic gain control (AGC): 1x10^{6} and 5x10^{4} for MS full scans and MS2,
237 respectively. The intensity threshold for MS2 was set to 1x10^{4}. Maximum fill times

238 were 50 ms (MS1) and 55 ms (MS2). Unassigned charge states, charged state 1 and

239 ions with charge state 5 and higher were rejected.

240

241 **Bioinformatic analyses**

242 LC-MS/MS data was processed with Proteome Discoverer (PD, version 2.2, Thermo

243 Fisher Scientific). Raw files were searched using the SequestHT algorithm against a

244 *P. patens* protein database based on the V1.6 gene models (Zimmer *et al.*, 2013)

245 supplemented with common contaminant proteins (cRAP, www.thegpm.org/crap/)

246 with the following settings: Precursor and fragment mass tolerances 10 ppm and

247 0.02 Da, respectively; minimum peptide length: 6; maximum of missed cleavages: 2;

248 variable modifications: Oxidation of methionine, N-acetylation of protein N-termini.

249 For the identification of ^{15}N-labelled peptides, a second database search was

250 performed with ^{14}N to ^{15}N substitution(s) set as static modifications for all amino

251 acids. Peptide-spectrum-matches (PSMs) were filtered using the Percolator node to

252 satisfy a false discovery rate of 0.01 (based on q-values). Identifications were filtered

253 to achieve a peptide and protein level FDR of 0.01. LC-MS/MS runs were

254 chromatographically aligned with a maximum retention time drift of 10 min. Precursor

255 ion quantification was performed using unique and razor peptides. Abundances were

256 normalized to the maximum total peptide abundance in all files. Protein ratios (Δ*gr1*

257 vs. WT) were calculated using the 'pairwise ratio based' approach with subsequent

258 hypothesis testing (background based t-test) for the calculation of p-values.

259 The mass spectrometry proteomics data have been deposited to the

260 ProteomeXchange Consortium (http://proteomecentral.proteomexchange.org) via the

261 PRIDE partner repository (Vizcaíno *et al.*, 2013) with the dataset identifier

262 <PXD012843>.

263

264 **NPQ measurements**

265 *In vivo* fluorescence in *P. patens* was measured with a Maxi-Imaging PAM

266 chlorophyll fluorometer (Heinz Walz). Before measurements, LL, CL and HL grown

267 protonema plates were dark-adapted for 40 min. NPQ (non-photochemical

268 quenching) was calculated as (Fm–Fm')/Fm'. Fv (the variable fluorescence) was

269 calculated as Fv=Fm–Fo. The Fv/Fm ratio was used to evaluate the maximum PSII

270 fluorescence in the fully dark-adapted state. Fm and Fm' represent the maximum

271 PSII fluorescence in the dark-adapted state and in any light-adapted state,

8

272 respectively, and Fo represents the minimum PSII fluorescence in the dark-adapted

273 state (Kukuczka *et al.*, 2014).

274

275 **Spectroscopic measurements of photosynthetic parameters**

276 Protonema from LL, CL and HL treated plates was measured with cellophane in

277 buffer (Hepes 20 mM pH 7.5, KCl 10 mM). LEF+CEF (linear plus cyclic electron flow)

278 and CEF (cyclic electron flow) were measured by following the relaxation kinetics of

279 the carotenoid electrochromic band shift at 520 nm (corrected by subtracting the

280 band shift at 546 nm) in the absence or presence of 10 µM DCMU and

281 hydroxylamine, respectively. CEF and LEF+CEF were calculated as $e^{-1}s^{-1}PSI^{-1}$ upon

282 normalization to the PSI amount. The electrochromic shift signal upon excitation with

283 a single saturating turnover flash (5 ns laser pulse) in the presence or absence of

284 10 µM DCMU and 1 mM hydroxylamine were used to estimate the PSI and PSI+PSII

285 amount. DCMU and hydroxylamine in this measurement were used to fully block PSII

286 photochemistry to facilitate the determination of the PSI amount (Terashima *et al.*,

287 2012; Gerotto *et al.*, 2016).

288 To measure the proton motive force (*pmf*), which consists of ∆pH (trans-thylakoid

289 proton gradient) and membrane potential (∆ψ), 5-day-old protonema tissue from

290 liquid cultures was harvested, dark-adapted for 15 min before analysis and exposed

291 for 1:30 h to 300 µmol photons m^{-2} s^{-1} to obtain the steady-state of the ECS signal.

292 Afterwards, a 1 min dark-phase was recorded (5 min of illumination in between

293 measurements) to obtain at least 3 technical replicates at 520 nm and 546 nm

294 respectively. g_H^+, which reflects the proton conductivity of the ATP synthase, was

295 estimated by fitting the first 300 ms of the decay curve with a first-order exponential

296 decay kinetic, ∆pH and ∆ψ were calculated as described previously (Wang *et al.*,

297 2015).

298

299 **Results**

300 **Moss lacking PpGR1 is viable and displays reduced growth**

301 Loss of plastidic GR in Arabidopsis leads to embryo lethality (L. Marty & A.J. Meyer,

302 unpublished), indicating an essential role in the non-photosynthetic tissues of early

303 sporophyte development, but also preventing further studies of GR function in green

304 tissues. We hence chose *Physcomitrella patens* as a model because knock-out

305 mutants can be generated using protoplastation and regeneration of

9

306 photosynthetically active vegetative cells, circumventing embryogenesis and non-
307 photosynthetic tissue (e.g. Schween *et al.* (2005)). We hypothesized that null
308 mutants of organellar GR might be viable in plants that maintain green plastids
309 throughout their life cycle. We therefore generated knock-out constructs replacing
310 exons two to five containing the translation start site and the active site in the gene
311 encoding the previously identified dual-targeted mitochondria and plastid-localised
312 glutathione reductase Pp1s13_127V6.1 (named *GR1* in *P. patens*, Xu *et al.*, (2013))
313 with a hygromycin resistance cassette via homologous recombination (Fig. S1a). As
314 genetic background, we utilised a newly generated *P. patens* line expressing the
315 plastid-targeted E_{GSH} biosensor Grx1-roGFP2 under the control of the *P. patens Actin*
316 *5* promoter (Weise *et al.*, 2006; Mueller & Reski, 2015). We isolated plants surviving
317 hygromycin selection under constant light. They were genotyped for the integration of
318 the knock-out construct at the target locus (Fig. S1b), and the absence of *PpGR1*
319 transcript was confirmed (Fig. S1c). All plants lacking *GR1* transcript showed a dwarf
320 phenotype (Fig. 1a) compared to the WT line and the line expressing plastid-targeted
321 Grx1-roGFP2 (cpGrx1roGFP2 #40, Fig.1a). Two independent lines, *Δgr1* #48 and
322 *Δgr1* #88, were chosen for further analysis. As the *Arabidopsis thaliana gr2-1* null
323 mutant is embryo-lethal, we tested if *Δgr1* knock-out mutants were able to complete
324 the moss life cycle. Under inducing conditions, *Δgr1* #48 and *Δgr1* #88 formed
325 sporophytes that underwent complete development and opened to release mature
326 spores (Fig. 1b). Thus, GR1 is not necessary for embryo development in *P. patens*.
327 However, spore germination of *Δgr1* #48 and Δgr1 #88 was delayed by several days,
328 with spores being able to germinate eventually (Fig. 1b). Apart from the dwarfed
329 appearance, the mutant lines grew fewer caulonema filaments and rhizoids than the
330 WT (Fig. S2).
331 The ultrastructure of chloroplasts lacking GR1 was investigated using transmission
332 electron microscopy (TEM), which revealed normally packed grana stacks and
333 stroma lamellae, undistinguishable from WT (Fig. S3).
334

335 **Plastid redox state is dynamic in WT, shifted to less reducing values in *Δgr1***
336 **plants and not rescued via Trx reduction under light**
337 Taking advantage of the stromal-targeted Grx1-roGFP2, the steady state of the
338 chloroplast E_{GSH} was determined by confocal *in vivo* imaging of roGFP2 redox state
339 (Fig. 2a). The fluorescence excitation ratio 405/488 nm ratio increases with sensor

10

340   oxidation. It was 0.91 +/- 0.17 in WT, 1.61 +/- 0.25 in *Δgr1*# 48 and 1.81 +/- 0.28 in

341   *Δgr1* #88 (Fig. 2a,b), indicating that the stromal E_{GSH} is less reducing in *Δgr1* lines. To

342   test for stability of stromal E_{GSH} after exogenous reduction, plants were incubated with

343   2 mM dithiothreitol (DTT) and then exposed to continuous laser scanning under the

344   confocal microscope. As a result, plastid Grx1-roGFP2 was rapidly re-oxidised in the

345   *Δgr1* plants, but not in the WT background (Fig. 2c). This result prompted us to

346   investigate the dynamics of E_{GSH} in dark-to-light and light-to-dark transitions (Fig. 2d).

347   Dark-adapted plants were exposed to a dark-to-light transition (100 µmol photons m^{-2}

348   s^{-1} for 10 min) during confocal imaging, resulting in a transient oxidation, followed by

349   a reduction of the Grx1-roGFP2 redox state. The following light-to-dark transition

350   (after 10 min of light exposure) resulted in an oxidation. Pre-incubation of plants with

351   the electron transport inhibitor 10 µM DCMU (3-(3,4-dichlorophenyl)-1,1-

352   dimethylurea) blocked the E_{GSH} dynamics, indicating a dependence on the

353   photosynthetic ETC. No reduction of Grx1-roGFP2 in the light was observed in *Δgr1*

354   plants. As Trx systems constitute a functional backup for cytosolic and mitochondrial

355   GRs (Marty *et al.*, 2009; L. Marty & A.J. Meyer, unpublished), we next investigated

356   whether the survival of *Δgr1* plants was dependent on the activity of the ferredoxin-

357   thioredoxin reductase (FTR) system. As FTR is supplied with electrons from the

358   chloroplast ETC, we tested survival of the *Δgr1* mutant lines after transfer from

359   constant light to short day conditions (Fig. S4a), and under extended darkness (44 d,

360   Fig. S4b). These experiments revealed that *Δgr1* #48 and *Δgr1* #88 were not

361   sensitive to incubation in darkness, suggesting that the FTR-dependent redox

362   cascades are not required for the survival of the *P. patens* mutants.

363

364   **_Δgr1_ plants show altered responses of reactive oxygen species dynamics and**

365   **photosynthetic function**

366   As *Δgr1* knock-out plants were not sensitive to dark-incubation (Fig. S4) and showed

367   an oxidative response to the laser light used for microscopic imaging (Fig. 2c), their

368   growth habit under different light intensities was tested (Fig. S5a). Mutants did not

369   profit from increasing light fluencies (30 to 130 µmol photons m^{-2} s^{-1}), as their fresh

370   weight did not increase, in contrast to WT (Fig. S5b). In order to investigate the

371   impact of different light intensities on ROS scavenging, the levels of ascorbate and

372   dehydroascorbate were determined. The measurements revealed a higher total level

373   of ascorbate in *Δgr1* #48 and *Δgr1* #88 that reached 500 % to 700 % of WT levels in

11

374 different light intensities (Fig. 3a). Interestingly, dehydroascorbate levels were
375 increased as well, but were present at the same ratio to reduced ascorbate as in WT
376 (on average 8.1+/-2.5 % of total ascorbate, Fig. 3b). We incubated gametophores
377 with nitro blue tetrazolium (NBT) in the dark or in light as a means to detect
378 superoxide ($O_2^{\cdot-}$), and found increased staining intensity in light-incubated *Δgr1*
379 plants (Fig. 3c). To induce additional ROS formation by photosystem I (PSI), single
380 gametophores were transferred to medium containing 1 μM Paraquat. While WT
381 plants were still able to grow, *Δgr1* #48 and *Δgr1* #88 plants bleached and died (Fig.
382 3d, upper panel). To stop photosynthetic electron flow, moss colonies were
383 transferred to photoheterotrophic growth conditions and their survival on DCMU was
384 tested according to Bricker *et al.* (2014). WT plants survived when sucrose (1% (w/v))
385 was present in the medium, whereas *Δgr1* #48 and *Δgr1* #88 plants bleached and
386 died (Fig. 3d, middle panel).

387 Under exposure to higher light fluencies (HL, 450 μmol photons m^{-2} s^{-1}), white sectors
388 appeared in leaflets of *Δgr1* plants (Fig. 4a). When HL was additionally combined
389 with elevated temperature *Δgr1* #48 and *Δgr1* #88 plants died, whereas WT and
390 *Δgr1* mutants were able to recover from temperature stress only (Fig. 4a). An
391 examination of photosynthetic parameters revealed a light intensity-dependent
392 decrease of non-photochemical quenching (NPQ), linear and cyclic photosynthetic
393 electron flow (LEF+CEF) and the photosystem I to photosystem II ratio (PSI/PSII)
394 (Fig. 4b). While the NPQ amplitude decreased with increasing light intensity in *Δgr1*,
395 the NPQ dark relaxation was slower under all light conditions tested. CEF was not
396 increased under different light intensities, but showed a slight increase after 6 h
397 induction via anoxia (Fig. S6a,b). The Fv/Fm ratio decreased in *Δgr1* with increasing
398 light, indicating decreased photosynthetic efficiency (Fig. S6a). At the same time,
399 total chlorophyll (a+b) levels were decreased (Fig. S6c).

400 To study the proton motive force (*pmf*) in mutant chloroplasts in comparison to WT,
401 electrochromic shift assays (Kramer & Crofts, 1989) were conducted and revealed a
402 decreased pH gradient and increased membrane potential ΔΨ in *Δgr1*, resulting in a
403 similar *pmf*. The proton conductivity of the ATP synthase was not significantly altered
404 (Fig. 4c).

405 As NPQ relaxation was slower under all light conditions tested, similar to Arabidopsis
406 *npq2* (zeaxanthin epoxidase) mutants (Niyogi *et al.*, 1998), we measured levels of
407 photosynthesis pigments and found that zeaxanthin levels were increased up to 2-

12

408 fold relative to total pigment content in the Δ*gr1* mutant in comparison to WT (Fig.

409 4d). Total glutathione levels (GSH+GSSG) were not significantly different to WT (Fig.

410 4e).

411

Quantitative proteomics reveals light intensity-dependent protein level

changes in Δ*gr1* plants

414 To assess the significance of GR function for proteostasis under changing light

415 intensities we used metabolic labelling with the stable isotope ^{15}N in combination with

416 quantitative proteomics. Changes in protein abundances in WT and Δ*gr1* plants upon

417 a shift from low light (LL) to high light (HL) were investigated using quantitative

418 proteomics (Fig. S7). The sensor expressing line cpGrx1roGFP2 #40 (WT) and

419 Δ*gr1#48* were labelled *in vivo* by growth on medium containing Ca(^{15}NO$_3$)$_2$ as

420 exclusive nitrogen source, or non ^{15}N-containing medium, respectively. Labelled and

421 unlabelled samples of both lines were exposed to HL and samples taken after 1 h

422 whereas control samples were kept at LL. For the same experimental condition,

423 protein extracts from labelled and unlabelled samples of Δ*gr1* and

424 cpGrx1roGFP2 #40 (WT), respectively, were mixed in a 1:1 ratio, tryptically digested

425 and analysed by LC-MS/MS. To exclude any bias introduced by the labelling, one

426 label swap experiment was performed per light intensity, resulting in a total of four

427 experiments (2x Δ*gr1* vs. WT HL, 2x Δ*gr1* vs. WT LL, Fig. S7). In total, 1657 proteins

428 with Δ*gr1* vs. WT ratios were quantified, of which 125 were differentially abundant

429 ($P<0.05$) in Δ*gr1* and WT in LL or HL (Fig. 5a, blue dots). Of these 125 proteins, 70

430 were down-regulated and 59 up-regulated (four were either up- or downregulated,

431 depending on the light conditions). The overlap between differentially regulated

432 proteins in LL in comparison to HL was 8.6 % for the down-regulated proteins and

433 20.3 % for the up-regulated proteins (Fig. 5b). Following a manual annotation of

434 subcellular localisation (Table S2), based on available organelle proteomics data sets

435 for *P. patens* (Mueller *et al.*, 2014) and SUBAcon (Hooper *et al.*, 2014) annotation of

436 Arabidopsis homologs, the largest fraction of regulated proteins was attributed to

437 plastids (38), followed by the cytosol (20) and proteins with unclear localisation (13)

438 (Fig. 5c). In addition, differentially regulated proteins were sorted into 29 functional

439 categories (Table S2) and categories containing more than two proteins plotted to

440 visualise category-specific down- or up-regulation in the different light conditions (Fig.

441 5d). Here, more proteins with unknown function were down-regulated specifically in

13

442   LL or HL whereas several proteins with unknown function were up-regulated in both

443   light conditions. In the categories "protein homeostasis" and "photosynthesis light

444   reactions" more proteins were down-regulated in LL, but more proteins were up-

445   regulated in HL, indicating a strong influence of the light intensity on protein levels in

446   these categories. PSI subunit E (Pp1s101_2V6.1, $2^{-0.33}$) was less abundant in LL,

447   whereas the plastid-encoded PSII subunits D1 and D2 were less abundant after the

448   shift to HL (PsbA PhpapaCp046, $2^{-0.25}$; PsbD PhpapaCp044, $2^{-0.2}$). In the functional

449   category "protein homeostasis", under HL, the increase of one isoform of the plastid

450   proteasome proteolytic subunit ClpP (Pp1s161_14V6.1, $2^{6.64}$) and of chaperonin 60

451   (Chp 60) alpha and beta subunits (Pp1s16_322V6.1 $2^{0.48}$; Pp1s14_298V6.1, $2^{0.47}$;

452   Pp1s15_485V6.1, $2^{0.55}$) indicated an increased demand for protein stabilization and

453   degradation. Proteins of cytosolic translation were down-regulated under LL,

454   whereas proteins of respiratory complex I and photosynthetic dark reactions were

455   only affected in HL. Proteins of plastid translation were up-regulated in LL.

456   Prominent changes in protein abundances include a plastid ribosome release factor

457   (Pp1s130_293V6.1, $2^{6.64}$, HL) and a KEA (K^+-efflux antiporter) homolog

458   (Pp1s2_217V6.1, $2^{-6.64}$, HL) with high similarity to AtKEA1 and AtKEA2 (Kunz *et al.*,

459   2014). Notably some enzyme isoforms were regulated differentially, such as enolase

460   (Pp1s1_527V6.1, c. $2^{1.2}$, LL+HL; Pp1s37_237V6.1, $2^{-6.64}$, LL+HL).

461   As PpGR1 (Pp1s13_127V6.1) was also identified in the proteomics analysis as

462   differentially abundant (Table S2), we confirmed the absence of PpGR1 additionally

463   by a targeted proteomics approach (Fig. S8).

464   Further, we screened the dataset for known redox-regulated proteins and found one

465   of the three isoforms of gamma subunit of chloroplast ATP synthase

466   (Pp1s35_234V6.1, $2^{-1.35}$, LL), a putative plastid glucose-6-phosphate dehydrogenase

467   (Pp1s338_65V6.1, $2^{-0.36}$, HL), as well as one of two FBPase isoforms (FBPase 2

468   Pp1s20_373V6.1 $2^{-0.87}$, HL) down-regulated. Interestingly, *P. patens* possesses a

469   putative oxidoreductase using GSSG with similarity to bacterial YfcG

470   (Pp1s339_37V6.1) that was down-regulated under both light conditions.

471

472   **Discussion**

473   **Stromal E_{GSH} responds to photosynthetic status**

474   We generated viable null mutants of *P. patens* GR1, and found that absence of GR1

475   leads to a shift in the stromal E_{GSH}. After Grx1-roGFP2 calibration, sensor 405/488

14

476   nm excitation ratio measurements can be translated into degree of sensor oxidation.

477   As the redox potential of roGFP2 equilibrates with the redox potential of glutathione,

478   E_{GSH} can be calculated, with the limitation that compartment pH has to be estimated

479   (Meyer *et al.*, 2007; Schwarzländer *et al.*, 2008). In *Δgr1* plants, the degree of

480   oxidation of the plastid-targeted E_{GSH} sensor Grx1-roGFP2 was severely shifted.

481   Based on the change of the 405/488 nm ratio and the *in vivo* sensor calibration (Fig.

482   2b), we calculated a shift from c. 48 % oxidation in the WT background to c. 92 %

483   oxidation in the *Δgr1* lines. This would correspond to a 33 mV shift in the redox

484   potential (calculated for pH8: -311 mV in WT vs. -278 mV in *Δgr1*). In comparison,

485   the redox potential in Arabidopsis epidermal plastids was determined as c. -361 mV

486   at pH 8 (Schwarzländer *et al.*, 2008). A shift of 30 mV would mean an increase of the

487   relative amount of GSSG from 0.01 % to 0.1 %, calculated for a total concentration of

488   2.5 mM GSH (Meyer *et al.*, 2007).

489   As in the same compartments glutathione- and Trx-dependent thiol switching fuelled

490   by distinct reductases co-exists (Buchanan & Balmer, 2005), the cross-talk of these

491   systems has been dissected for the cytosol and the mitochondria. Thus, cytosolic Trx

492   redox-state can be rescued via the glutathione system (Reichheld *et al.*, 2007). Vice

493   versa, the NTRA/B system present in the cytosol and the mitochondria constitutes a

494   functional backup of the glutathione system (Marty *et al.*, 2009). However, reduction

495   of many plastid Trxs is light-dependent and E_{GSH} in other cellular compartments is

496   stable. It was hypothesized that the Trx-dependent redox cascades in plastids cannot

497   provide sufficient backup to reduce the plastid E_{GSH} (L. Marty & A.J. Meyer,

498   unpublished). Our data indicate that a shift of E_{GSH} in plastids occurs in the absence

499   of GR, but that this shift is limited. The resulting steady state level may be a

500   consequence of either electron flux to GSSG from Trxs, export of GSSG (Morgan *et*

501   *al.*, 2013; Noctor *et al.*, 2013) from plastids or increased GSH biosynthesis

502   (Choudhury *et al.*, 2018). However, we did not find increased glutathione levels in the

503   absence of GR1 (Fig. 4e). In dynamic measurements in ectopically reduced *Δgr1*

504   plants, the shifted stromal E_{GSH} was rapidly re-established by exposure to laser light,

505   suggesting that GSSG rapidly accumulates in mutants upon illumination. As the

506   regeneration of GSSG via GR is lacking in the mutant plastids, this likely represents

507   GSSG formed by the ascorbate-GSH cycle, i.e. dehydroascorbate reductase (DHAR)

508   activity. While the relative contributions of monodehydroascorbate reductase

509   (MDHAR) and DHAR to the plastid ascorbate regeneration were debated (Asada,

15

510 1999; Polle, 2001), plastid-targeted AtDHAR3 was shown to contribute to ascorbate

511 recycling with mutants being sensitive to high light (Noshi *et al.*, 2016). The increase

512 in total ascorbate and dehydroascorbate levels in $\Delta gr1$ mutants indicates impaired

513 function of the ascorbate-GSH cycle consistent with a substantial contribution of

514 plastid GR, including non-stress conditions. Light was not necessary for the survival

515 of $\Delta gr1$ plants, indicating that light-dependent reduction of Trxs was not a

516 prerequisite for viability. Further, cross-talk between the Trx- and glutathione redox

517 cascades in plastids is limited, which is in contrast to previous findings in the cytosol

518 and mitochondria (Reichheld *et al.*, 2007; Marty *et al.*, 2009).

519 Notably, in WT plants exposed to a successive dark/light and light/dark transition, the

520 stromal E_{GSH} responded dynamically, showing that E_{GSH} is rapidly light-responsive in

521 the presence of GR. In addition, after the transition from light to darkness, we

522 observed a rapid rise of the stromal E_{GSH} pointing to oxidative processes in

523 consequence of a light/dark transition. This oxidation is analogous to Trx oxidation

524 that is required to deactivate redox-regulated Calvin Benson cycle enzymes

525 (Wolosiuk & Buchanan, 1977; Yoshida *et al.*, 2018). Peroxiredoxins have been

526 reported to act as possible electron sinks (Pérez-Ruiz *et al.*, 2017; Vaseghi *et al.*,

527 2018).

528 At the measured stromal E_{GSH} in $\Delta gr1$, still most of the stromal glutathione is present

529 in the reduced state (99.9 %). Nevertheless, a shifted E_{GSH} is likely to affect

530 downstream redox-cascades, as well as GSH-dependent enzymatic reactions. This

531 includes glutaredoxins (Grx) and dehydroascorbate reductase (DHAR). While the

532 involvement of plastid Grxs in iron-sulfur cluster coordination and protein

533 (de)glutathionylation has been shown (Zaffagnini *et al.*, 2012; Moseler *et al.*, 2015;

534 Rey *et al.*, 2017; Zannini *et al.*, 2019), only very few target proteins are currently

535 known. Thus, the future challenge is to identify specific target cysteines affected by a

536 shifting E_{GSH} in order to appraise its potential physiological role in redox regulation

537 and signalling.

538

Consequences of a lack in plastid/mitochondrial GR

540 The absence of plastid/mitochondrial GR resulted in a pronounced dwarfism as well

541 as in light sensitivity of the mutant plants. As dual targeting of one GR isoform is

542 evolutionarily conserved (Xu *et al.*, 2013), the contribution of the lack of mitochondrial

543 GR to the overall phenotype of the mutants is not resolved yet. However, in

16

544   Arabidopsis it is the lack of GR in plastids, and not in mitochondria, that results in
545   embryo-lethality (L. Marty & A.J. Meyer, unpublished; Nietzel *et al.*, 2019). We found
546   that in *P. patens*, the plastid/mitochondrial isoform of GR is not necessary for embryo
547   development. This suggests that either (1) the process that causes embryo-lethality
548   in Arabidopsis is not important for *P. patens* embryo development, or (2) that the lack
549   of GR is compensated for in *P. patens* allowing embryo development to proceed. For
550   instance, in contrast to flowering plant *gr* mutants under stress (Ding *et al.*, 2012),
551   *P. patens Δgr1* mutants showed a high increase in total ascorbate levels.

552   In the green haploid moss gametophyte, lack of GR1 caused slow growth as well as
553   defects in photosynthetic parameters. Whereas photosynthetic electron flow was not
554   affected in low light, increasing light fluencies resulted in decreased electron flow in
555   photosynthetic light reactions, as well as a near complete loss of NPQ. In addition,
556   the retarded relaxation of NPQ kinetics and increased zeaxanthin levels, similar to
557   the Arabidopsis *npq2* mutant lacking zeaxanthin epoxidase (Niyogi *et al.*, 1998)
558   suggest an influence of E_{GSH} in the regulation of zeaxanthin epoxidase, also under
559   non-stress conditions. Under HL, violaxanthin is converted into zeaxanthin which is
560   involved in scavenging ROS as inferred from the analysis of Arabidopsis *vte1* mutant
561   deficient in the synthesis of tocopherol, one of the lipid antioxidants in chloroplasts
562   (Havaux *et al.*, 2005). Violaxanthin de-epoxidase, the enzyme involved in zeaxanthin
563   production, is activated by acidification of the lumen pH and uses ascorbate as
564   cosubstrate (Arnoux *et al.*, 2009).

565   Further, an increasing PSI/PSII ratio under higher light fluencies indicated PSII
566   damage. Concomitantly, we found decreased levels of photosystem II subunits
567   D1/D2 and increased protein levels of plastid chaperones and protein degradation,
568   confirming an increased demand for protein repair and degradation in HL. PSII
569   efficiency was already linked to GR activity in a study using a tobacco line with 30 %
570   of plastid/mitochondrial GR activity (Ding *et al.*, 2009). Here, the diminished GR
571   activity resulted in decreased chlorophyll, ascorbate, DHA levels and PSII efficiency,
572   as well as increased H_2O_2 levels under chilling stress (Ding *et al.*, 2012).
573   Concomitantly, overexpression of plastid/mitochondrial GR was beneficial under
574   photoinhibitory conditions in poplar and cotton (Foyer *et al.*, 1995; Kornyeyev *et al.*,
575   2003).

576   In *Δgr1* plants, we found an elevated ∆ψ and decreased ∆pH, resulting in a similar
577   *pmf* and H$^+$ conductivity ($g_H{}^+$) compared to WT. An elevated electric field component

17

578   can increase PSII photodamage (Davis *et al.*, 2016). In addition, we found increased

579   sensitivity to ROS, as well as increased superoxide tissue staining in the Δ*gr1*

580   mutant. The chloroplasts possess a very efficient removal system for ROS, with

581   several ascorbate peroxidases that detoxify hydrogen peroxide using ascorbate as

582   an electron donor. On the other hand, ascorbate peroxidases represent themselves

583   prominent targets for ROS-induced damage (Dietz, 2016). Therefore, it is possible

584   that the higher ROS fluxes reached in the Δ*gr1* plants, even under non-stress

585   conditions, leads to decreased enzymatic ascorbate peroxidation and increased

586   ROS-induced damage. Further, ROS inhibit plastid translation and thereby PSII

587   repair (Nishiyama *et al.*, 2011). In tobacco, 30 % of plastid GR activity was sufficient

588   to avoid ROS formation under non-stress conditions (Ding *et al.*, 2009). Our data

589   clearly indicate that the presence of functional PSII in increasing light intensities is

590   linked to a highly reducing stromal $E_{GSH.}$

591   Only a low percentage of quantified protein differed in protein abundance between

592   Δ*gr1* and WT plants in LL and after a shift from LL to HL (7.5 %, 125 of 1657). The

593   affected proteins are distributed across several compartments, with the plastid being

594   the most prominent localisation (30 %), confirming the important role of GR for plastid

595   processes. The impact also on cytosolic proteins shows that the mutant cells adjust

596   their protein content to the altered situation in the chloroplasts, possibly suggesting

597   active retrograde signalling between chloroplast and nucleus. Notably, after the shift

598   to HL, also mitochondrial proteins (3 complex I subunits) became affected,

599   suggesting a role of mitochondrial GR under HL conditions.

600   Following manual annotation of proteins and allocation to process categories several

601   patterns became apparent. Proteins involved in cytosolic translation were mostly less

602   abundant in Δ*gr1* plants, while several proteins from plastid translation were more

603   abundant. In addition, proteins of plastid glycolysis and fatty acid biosynthesis as well

604   as proteolysis- and protein folding-related proteins were more abundant in Δ*gr1*

605   plants. Adjustment of several photosynthesis-related proteins was already apparent

606   in LL, confirming that GR function is not only relevant under stress conditions.

607   In HL, altered levels of transport proteins such as the inner envelope H^+/K^+ antiporter

608   (KEA) isoform may contribute to phenotypes such as decreased ∆pH within the *pmf*

609   component in Δ*gr1* mutants (Kunz *et al.*, 2014). Interestingly, plant KEA isoforms

610   possess sequence similarity to the glutathione-regulated potassium-efflux system

611   KefC of *Escherichia coli* (Roosild *et al.*, 2010). This system is important for protection

612 against toxic electrophiles via acidification (Ferguson, 1999) and is negatively
613 regulated by GSH, but activated by glutathione conjugates (Roosild *et al.*, 2010). It is
614 tempting to speculate that activity or abundance of plant KEA isoforms in the inner
615 plastid envelope are linked to changes in stromal glutathione redox state. In the
616 absence of AtKEA1/2 NPQ decreased and PSII was compromised (Kunz *et al.*,
617 2014), which is line with the Δ*gr1* data. In contrast, deletion of the thylakoid localized
618 H$^+$/K$^+$ antiporter AtKEA3 resulted in high NPQ in Arabidopsis (Armbruster *et al.*, 2014;
619 Wang *et al.*, 2017). As stated above, analyses of *pmf* partitioning between ΔΨ and
620 ΔpH revealed a decrease in the putative ΔpH component. Notably, the ΔpH
621 component could be also modulated by ATP hydrolysis/formation in the dark until
622 equilibrium between the *pmf* and the phosphorylating potential is reached (Cruz *et*
623 *al.*, 2001; Allorent *et al.*, 2018). Considering the less reducing stromal E_{GSH} in Δ*gr1*, a
624 difference in phosphorylating potential between WT and Δ*gr1* is possible, which
625 could also explain differences in the putative ΔpH component.

626 Notably, the abundance of several known redox-regulated proteins was decreased in
627 absence of GR1, such as one FBPase isoform and the chloroplast ATP-synthase
628 gamma subunit. It is tempting to speculate that cysteines may become over-oxidised
629 in Δ*gr1* plants, leading to changes in protein activity or to protein degradation (De
630 Smet *et al.*, 2019; Zaffagnini *et al.*, 2019).

631

632 In conclusion the overall phenotype of Δ*gr1* mutants is likely a mixture of different
633 effects: direct consequences via E_{GSH} and protein mis-regulation, and indirect
634 consequences via ROS-induced protein damage. Investigations of cysteine redox
635 state, GSH metabolites, glutathionylation of proteins and redox-cascades
636 downstream of plastid/mitochondrial E_{GSH} provide scope for future research.

637

19

646 PAK918) including the grants SCHW1719/5-1 and MU4137/1-1. M.H. acknowledges

647 funding by the Deutsche Forschungsgemeinschaft (DFG, HI 739/13-1). Research in

648 S.K.´s laboratory is funded by DFG (EXC1028).

649 We thank Bastian Welter (University of Cologne) and Alexa Brox (INRES, University

650 of Bonn) for technical assistance.

651

Author Contributions

653 S.J.M.S., P.D., M.Schw., R.R., M.H. and A.J.M. planned and designed the research.

654 S.J.M.S., R.W., D.D.G., J.R., S.K., M.R., V.L. performed experiments. M.Scho.

655 analysed data. S.J.M.S. and A.J.M. wrote the manuscript. All authors discussed data

656 and approved the final version of the manuscript.

657

References

659 **Allorent, G., Byrdin, M., Carraretto, L., Morosinotto, T., Szabo, I., & Finazzi, G**.
660 **2018**. Global spectroscopic analysis to study the regulation of the photosynthetic
661 proton motive force: A critical reappraisal. *Biochimica et Biophysica Acta (BBA)-*
662 *Bioenergetics* **1859**: 676-683.

663 **Armbruster U, Carrillo LR, Venema K, Pavlovic L, Schmidtmann E, Kornfeld A,**
664 **Jahns P, Berry JA, Kramer DM, Jonikas MC**. **2014**. Ion antiport accelerates
665 photosynthetic acclimation in fluctuating light environments. *Nature Communications*
666 **5**: 5439.

667 **Arnoux P, Morosinotto T, Saga G, Bassi R, Pignol D**. **2009**. A structural basis for
668 the pH-dependent xanthophyll cycle in *Arabidopsis thaliana*. *The Plant Cell* **21**:
669 2036–2044.

670 **Asada K**. **1999**. The water-water cycle in chloroplasts: Scavenging of active oxygens
671 and dissipation of excess photons. *Annual Review of Plant Physiology and Plant*
672 *Molecular Biology* **50**: 601–639.

673 **Bricker TM, Bell AJ, Tran L, Frankel LK, Theg SM**. **2014**. Photoheterotrophic
674 growth of *Physcomitrella patens*. *Planta* **239**: 605–613.

675 **Buchanan BB, Balmer Y**. **2005**. Redox regulation: A broadening horizon. *Annual*
676 *Review of Plant Biology* **56**: 187–220.

677 **Choudhury FK, Devireddy AR, Azad RK, Shulaev V, Mittler R**. **2018**. Rapid
678 accumulation of glutathione during light stress in *Arabidopsis*. *Plant & Cell*
679 *Physiology* **59**: 1817-1826.

680 **Cruz JA, Sacksteder CA, Kanazawa A, Kramer DM**. **2001**. Contribution of electric
681 field (Δψ) to steady-state transthylakoid proton motive force (*pmf*) *in vitro* and *in vivo*.
682 Control of *pmf* parsing into Δψ and ΔpH by ionic strength. *Biochemistry* **40**: 1226–
683 1237.

20

Davis GA, Kanazawa A, Schöttler MA, Kohzuma K, Froehlich JE, Rutherford AW, Satoh-Cruz M, Minhas D, Tietz S, Dhingra A, *et al.* 2016. Limitations to photosynthesis by proton motive force-induced photosystem II photodamage. *eLife* **5**: e16921.

De Smet B, Willems P, Fernandez-Fernandez AD, Alseekh S, Fernie AR, Messens J, Van Breusegem F. **2019**. *In vivo* detection of protein cysteine sulfenylation in plastids. *The Plant Journal* **97**:765-778*.*

Dietz K-J. **2016**. Thiol-based peroxidases and ascorbate peroxidases: Why plants rely on multiple peroxidase systems in the photosynthesizing chloroplast? *Molecules and Cells* **39**: 20–25.

Dietz K-J, Turkan I, Krieger-Liszkay A. **2016**. Redox- and reactive oxygen species-dependent signalling in and from the photosynthesizing chloroplast. *Plant Physiology* **171**: 1541-1550.

Ding S, Lei M, Lu Q, Zhang A, Yin Y, Wen X, Zhang L, Lu C. **2012**. Enhanced sensitivity and characterization of photosystem II in transgenic tobacco plants with decreased chloroplast glutathione reductase under chilling stress. *Biochimica et Biophysica Acta* **1817**: 1979–1991.

Ding S, Lu Q, Zhang Y, Yang Z, Wen X, Zhang L, Lu C. **2009**. Enhanced sensitivity to oxidative stress in transgenic tobacco plants with decreased glutathione reductase activity leads to a decrease in ascorbate pool and ascorbate redox state. *Plant Molecular Biology* **69**: 577–592.

Egener T, Granado J, Guitton MC, Hohe A, Holtorf H, Lucht JM, Rensing SA, Schlink K, Schulte J, Schween G, *et al.* 2002. High frequency of phenotypic deviations in *Physcomitrella patens* plants transformed with a gene-disruption library. *BMC Plant Biology* **2**: 6.

Ferguson GP. **1999**. Protective mechanisms against toxic electrophiles in *Escherischia coli*. *Trends in Microbiology* **7**: 242–247.

Foyer CH, Noctor G. **2011**. Ascorbate and glutathione: The heart of the redox hub. *Plant Physiology* **155**: 2–18.

Foyer CH, Souriau N, Perret S, Lelandais M, Kunert KJ, Pruvost C, Jouanin L. **1995**. Overexpression of glutathione reductase but not glutathione synthetase leads to increases in antioxidant capacity and resistance to photoinhibition in poplar trees. *Plant Physiology* **109**: 1047–1057.

Fricker MD. **2016**. Quantitative redox imaging software. *Antioxidants & Redox Signaling* **24**: 752–762.

Geigenberger P, Thormählen I, Daloso DM, Fernie AR. **2017**. The unprecedented versatility of the plant thioredoxin system. *Trends in Plant Science* **22**: 249–262.

Gerotto C, Alboresi A, Meneghesso A, Jokel M, Suorsa M, Aro E-M, Morosinotto T. **2016**. Flavodiiron proteins act as safety valve for electrons in *Physcomitrella patens*. *Proceedings of the National Academy of Sciences of the United States of America* **113**: 12322–12327.

21

725 **Gillespie KM, Ainsworth EA**. **2007**. Measurement of reduced, oxidized and total
726 ascorbate content in plants. *Nature Protocols* **2**: 871–874.

727 **Gütle DD, Roret T, Hecker A, Reski R, Jacquot J-P**. **2017**. Dithiol disulphide
728 exchange in redox regulation of chloroplast enzymes in response to evolutionary and
729 structural constraints. *Plant Science* **255**: 1–11.

730 **Havaux M, Eymery F, Porfirova S, Rey P, Dörmann P**. **2005**. Vitamin E protects
731 against photoinhibition and photooxidative stress in *Arabidopsis thaliana*. *The Plant*
732 *Cell* **17**: 3451–3469.

733 **Hohe A, Egener T, Lucht JM, Holtorf H, Reinhard C, Schween G, Reski R**. **2004**.
734 An improved and highly standardised transformation procedure allows efficient
735 production of single and multiple targeted gene-knockouts in a moss, *Physcomitrella*
736 *patens*. *Current Genetics* **44**: 339–347.

737 **Hooper CM, Tanz SK, Castleden IR, Vacher MA, Small ID, Millar AH**. **2014**.
738 SUBAcon: a consensus algorithm for unifying the subcellular localization data of the
739 *Arabidopsis* proteome. *Bioinformatics (Oxford, England)* **30**: 3356–3364.

740 **Hulsen T, de Vlieg J, Alkema W**. **2008**. BioVenn - a web application for the
741 comparison and visualization of biological lists using area-proportional Venn
742 diagrams. *BMC Genomics* **9**: 488.

743 **Kojer K, Bien M, Gangel H, Morgan B, Dick TP, Riemer J**. **2012**. Glutathione redox
744 potential in the mitochondrial intermembrane space is linked to the cytosol and
745 impacts the Mia40 redox state. *The EMBO Journal* **31**: 3169–3182.

746 **Kornyeyev D, Logan BA, Payton PR, Allen RD, Holaday AS**. **2003**. Elevated
747 chloroplastic glutathione reductase activities decrease chilling-induced
748 photoinhibition by increasing rates of photochemistry, but not thermal energy
749 dissipation, in transgenic cotton. *Functional Plant Biology* **30**: 101.

750 **Kramer DM, Crofts AR**. **1989**. Activation of the chloroplast ATPase measured by the
751 electrochromic change in leaves of intact plants. *Biochimica et Biophysica Acta*
752 *(BBA) - Bioenergetics* **976**: 28–41.

753 **Kubo M, Imai A, Nishiyama T, Ishikawa M, Sato Y, Kurata T, Hiwatashi Y, Reski**
754 **R, Hasebe M**. **2013**. System for stable β-estradiol-inducible gene expression in the
755 moss *Physcomitrella patens*. *PloS One* **8**: e77356.

756 **Kukuczka B, Magneschi L, Petroutsos D, Steinbeck J, Bald T, Powikrowska M,**
757 **Fufezan C, Finazzi G, Hippler M**. **2014**. Proton gradient regulation5-like1-mediated
758 cyclic electron flow is crucial for acclimation to anoxia and complementary to
759 nonphotochemical quenching in stress adaptation. *Plant Physiology* **165**: 1604–1617.

760 **Kunz H-H, Gierth M, Herdean A, Satoh-Cruz M, Kramer DM, Spetea C,**
761 **Schroeder JI**. **2014**. Plastidial transporters KEA1, -2, and -3 are essential for
762 chloroplast osmoregulation, integrity, and pH regulation in *Arabidopsis*. *Proceedings*
763 *of the National Academy of Sciences* **111**: 7480–7485.

764 **Lee B, Lee H, Xiong L, Zhu J-K**. **2002**. A mitochondrial complex I defect impairs
765 cold-regulated nuclear gene expression. *The Plant Cell* **14**: 1235–1251.

22

766 **Marty L, Siala W, Schwarzlander M, Fricker MD, Wirtz M, Sweetlove LJ, Meyer Y,**
767 **Meyer AJ, Reichheld J-P, Hell R**. **2009**. The NADPH-dependent thioredoxin system
768 constitutes a functional backup for cytosolic glutathione reductase in *Arabidopsis*.
769 *Proceedings of the National Academy of Sciences* **106**: 9109–9114.

770 **Meyer AJ**. **2008**. The integration of glutathione homeostasis and redox signaling.
771 *Journal of Plant Physiology* **165**: 1390–1403.

772 **Meyer Y, Belin C, Delorme-Hinoux V, Reichheld J-P, Riondet C**. **2012**.
773 Thioredoxin and glutaredoxin systems in plants: molecular mechanisms, crosstalks,
774 and functional significance. *Antioxidants & Redox Signaling* **17**: 1124–1160.

775 **Meyer AJ, Brach T, Marty L, Kreye S, Rouhier N, Jacquot J-P, Hell R**. **2007**.
776 Redox-sensitive GFP in *Arabidopsis thaliana* is a quantitative biosensor for the redox
777 potential of the cellular glutathione redox buffer. *The Plant Journal* **52**: 973–986.

778 **Meyer AJ, May MJ, Fricker M**. **2001**. Quantitative *in vivo* measurement of
779 glutathione in *Arabidopsis* cells. *The Plant Journal* **27**: 67–78.

780 **Morgan B, Ezeriņa D, Amoako TNE, Riemer J, Seedorf M, Dick TP**. **2013**. Multiple
781 glutathione disulfide removal pathways mediate cytosolic redox homeostasis. *Nature*
782 *Chemical Biology* **9**: 119–125.

783 **Moseler A, Aller I, Wagner S, Nietzel T, Przybyla-Toscano J, Mühlenhoff U, Lill**
784 **R, Berndt C, Rouhier N, Schwarzländer M, et al.** **2015**. The mitochondrial
785 monothiol glutaredoxin S15 is essential for iron-sulfur protein maturation in
786 *Arabidopsis thaliana*. *Proceedings of the National Academy of Sciences of the United*
787 *States of America* **112**: 13735–13740.

788 **Mueller SJ, Lang D, Hoernstein SNW, Lang EGE, Schuessele C, Schmidt A,**
789 **Fluck M, Leisibach D, Niegl C, Zimmer AD, et al.** **2014**. Quantitative analysis of the
790 mitochondrial and plastid proteomes of the moss *Physcomitrella patens* reveals
791 protein macrocompartmentation and microcompartmentation. *Plant Physiology* **164**:
792 2081–2095.

793 **Mueller SJ, Reski R**. **2015**. Mitochondrial dynamics and the ER: The plant
794 perspective. *Frontiers in Cell and Developmental Biology* **3**: 78.

795 **Nietzel T, Elsässer M, Ruberti C, Steinbeck J, Ugalde JM, Fuchs P, Wagner S,**
796 **Ostermann L, Moseler A, Lemke P, et al**. **2019**. The fluorescent protein sensor
797 roGFP2-Orp1 monitors *in vivo* H_2O_2 and thiol redox integration and elucidates
798 intracellular H_2O_2 dynamics during elicitor-induced oxidative burst in *Arabidopsis*.
799 *New Phytologist* **221**: 1649-1664.

800 **Nishiyama Y, Allakhverdiev SI, Murata N**. **2011**. Protein synthesis is the primary
801 target of reactive oxygen species in the photoinhibition of photosystem II. *Physiologia*
802 *Plantarum* **142**: 35–46.

803 **Niyogi KK, Grossman AR, Björkman O**. **1998**. *Arabidopsis* mutants define a central
804 role for the xanthophyll cycle in the regulation of photosynthetic energy conversion.
805 *The Plant Cell* **10**: 1121–1134.

Noctor G, Mhamdi A, Queval G, Foyer CH. **2013**. Regulating the redox gatekeeper: vacuolar sequestration puts glutathione disulfide in its place. *Plant Physiology* **163**: 665–671.

Noshi M, Hatanaka R, Tanabe N, Terai Y, Maruta T, Shigeoka S. **2016**. Redox regulation of ascorbate and glutathione by a chloroplastic dehydroascorbate reductase is required for high-light stress tolerance in *Arabidopsis*. *Bioscience, Biotechnology, and Biochemistry* **80**: 870–877.

Pérez-Ruiz JM, Naranjo B, Ojeda V, Guinea M, Cejudo FJ. **2017**. NTRC-dependent redox balance of 2-Cys peroxiredoxins is needed for optimal function of the photosynthetic apparatus. *Proceedings of the National Academy of Sciences of the United States of America* **114**: 12069-12074.

Polle A. **2001**. Dissecting the superoxide dismutase-ascorbate-glutathione-pathway in chloroplasts by metabolic modeling. Computer simulations as a step towards flux analysis. *Plant Physiology* **126**: 445–462.

Reichheld J-P, Khafif M, Riondet C, Droux M, Bonnard G, Meyer Y. **2007**. Inactivation of thioredoxin reductases reveals a complex interplay between thioredoxin and glutathione pathways in *Arabidopsis* development. *The Plant Cell* **19**: 1851–1865.

Reski R. **2018**. Quantitative moss cell biology. *Current Opinion in Plant Biology* **46**: 39–47.

Reski R, Abel WO. **1985**. Induction of budding on chloronemata and caulonemata of the moss, *Physcomitrella patens*, using isopentenyladenine. *Planta* **165**: 354–358.

Rey P, Becuwe N, Tourrette S, Rouhier N. **2017**. Involvement of *Arabidopsis* glutaredoxin S14 in the maintenance of chlorophyll content. *Plant, Cell & Environment* **40**: 2319-2332.

Roosild TP, Castronovo S, Healy J, Miller S, Pliotas C, Rasmussen T, Bartlett W, Conway SJ, Booth IR. **2010**. Mechanism of ligand-gated potassium efflux in bacterial pathogens. *Proceedings of the National Academy of Sciences of the United States of America* **107**: 19784–19789.

Schöttler MA, Toth SZ. **2014**. Photosynthetic complex stoichiometry dynamics in higher plants: Environmental acclimation and photosynthetic flux control. *Frontiers in Plant Science* **5**: 188.

Schuessele C, Hoernstein SNW, Mueller SJ, Rodriguez-Franco M, Lorenz T, Lang D, Igloi GL, Reski R. **2016**. Spatio-temporal patterning of arginyl-tRNA protein transferase (ATE) contributes to gametophytic development in a moss. *The New Phytologist* **209**: 1014–1027.

Schwarzländer M, Finkemeier I. **2013**. Mitochondrial energy and redox signaling in plants. *Antioxidants & redox signaling* **18**: 2122–2144.

Schwarzländer M, Fricker MD, MüLler C, Marty L, Brach T, Novak J, Sweetlove LJ, Hell R, Meyer AJ. **2008**. Confocal imaging of glutathione redox potential in living plant cells. *Journal of Microscopy* **231**: 299–316.

24

847 **Schween G, Egener T, Fritzowsky D, Granado J, Guitton M-C, Hartmann N,**
848 **Hohe A, Holtorf H, Lang D, Lucht JM, *et al.* 2005**. Large-scale analysis of 73 329
849 *Physcomitrella plants* transformed with different gene disruption libraries: Production
850 parameters and mutant phenotypes. *Plant Biology (Stuttgart, Germany)* **7**: 228–237.

851 **Speiser A, Silbermann M, Dong Y, Haberland S, Uslu VV, Wang S, Bangash**
852 **SAK, Reichelt M, Meyer AJ, Wirtz M, *et al.* 2018**. Sulfur partitioning between
853 glutathione and protein synthesis determines plant growth. *Plant Physiology* **177**:
854 927-937.

855 **Suzuki N, Koussevitzky S, Mittler R, Miller G**. **2012**. ROS and redox signalling in
856 the response of plants to abiotic stress: ROS and redox signalling in plants. *Plant,*
857 *Cell & Environment* **35**: 259–270.

858 **Terashima M, Petroutsos D, Hüdig M, Tolstygina I, Trompelt K, Gäbelein P,**
859 **Fufezan C, Kudla J, Weinl S, Finazzi G, *et al.* 2012**. Calcium-dependent regulation
860 of cyclic photosynthetic electron transfer by a CAS, ANR1, and PGRL1 complex.
861 *Proceedings of the National Academy of Sciences of the United States of America*
862 **109**: 17717–17722.

863 **Thayer SS, Björkman O**. **1990**. Leaf Xanthophyll content and composition in sun
864 and shade determined by HPLC. *Photosynthesis Research* **23**: 331–343.

865 **Vaseghi M-J, Chibani K, Telman W, Liebthal MF, Gerken M, Schnitzer H, Mueller**
866 **SM, Dietz K-J**. **2018**. The chloroplast 2-cysteine peroxiredoxin functions as
867 thioredoxin oxidase in redox regulation of chloroplast metabolism. *eLife* **7**: e38194.

868 **Vizcaíno JA, Côté RG, Csordas A, Dianes JA, Fabregat A, Foster JM, Griss J,**
869 **Alpi E, Birim M, Contell J, *et al.* 2013**. The PRoteomics IDEntifications (PRIDE)
870 database and associated tools: status in 2013. *Nucleic Acids Research* **41**: D1063-
871 1069.

872 **Wang C, Yamamoto H, Narumiya F, Munekage YN, Finazzi G, Szabo I, Shikanai**
873 **T**. **2017**. Fine-tuned regulation of the K+/H +antiporter KEA3 is required to optimize
874 photosynthesis during induction. *The Plant Journal* **89**: 540–553.

875 **Wang C, Yamamoto H, Shikanai T**. **2015**. Role of cyclic electron transport around
876 photosystem I in regulating proton motive force. *Biochimica et Biophysica Acta* **1847**:
877 931–938.

878 **Weise A, Rodriguez-Franco M, Timm B, Hermann M, Link S, Jost W, Gorr G**.
879 **2006**. Use of *Physcomitrella patens* actin 5' regions for high transgene expression:
880 importance of 5' introns. *Applied Microbiology and Biotechnology* **70**: 337–345.

881 **Wiśniewski JR, Zougman A, Nagaraj N, Mann M**. **2009**. Universal sample
882 preparation method for proteome analysis. *Nature Methods* **6**: 359–362.

883 **Wolosiuk RA, Buchanan BB**. **1977**. Thioredoxin and glutathione regulate
884 photosynthesis in chloroplasts. *Nature* **266**: 565–567.

885 **Xu L, Carrie C, Law SR, Murcha MW, Whelan J**. **2013**. Acquisition, conservation,
886 and loss of dual-targeted proteins in land plants. *Plant Physiology* **161**: 644–662.

25

887 **Yoshida K, Hara A, Sugiura K, Fukaya Y, Hisabori T**. **2018**. Thioredoxin-like2/2-
888 Cys peroxiredoxin redox cascade supports oxidative thiol modulation in chloroplasts.
889 *Proceedings of the National Academy of Sciences of the United States of America*
890 **115**: E8296-E8304.

891 **Yoshida K, Hisabori T**. **2016**. Two distinct redox cascades cooperatively regulate
892 chloroplast functions and sustain plant viability. *Proceedings of the National*
893 *Academy of Sciences of the United States of America* **113**: E3967-E3976.

894 **Yu X, Pasternak T, Eiblmeier M, Ditengou F, Kochersperger P, Sun J, Wang H,**
895 **Rennenberg H, Teale W, Paponov I,** *et al.* **2013**. Plastid-localized glutathione
896 reductase2-regulated glutathione redox status is essential for *Arabidopsis* root apical
897 meristem maintenance. *The Plant Cell* **25**: 4451–4468.

898 **Zaffagnini M, Bedhomme M, Marchand CH, Morisse S, Trost P, Lemaire SD**.
899 **2012**. Redox regulation in photosynthetic organisms: Focus on glutathionylation.
900 *Antioxidants & Redox Signaling* **16**: 567–586.

901 **Zaffagnini M, Fermani S, Marchand CH, Costa A, Sparla F, Rouhier N,**
902 **Geigenberger P, Lemaire SD, Trost P**. **2019**. Redox homeostasis in photosynthetic
903 organisms: Novel and established thiol-based molecular mechanisms. *Antioxidants &*
904 *Redox Signaling* doi: 10.1089/ars.2018.7617

905 **Zannini F, Moseler A, Bchini R, Dhalleine T, Meyer AJ, Rouhier N, Couturier J**.
906 **2019**. The thioredoxin-mediated recycling of *Arabidopsis thaliana* GRXS16 relies on
907 a conserved C-terminal cysteine. *Biochimica et Biophysica Acta (BBA)-General*
908 *Subjects* **1863**: 426-436.

909 **Zimmer AD, Lang D, Buchta K, Rombauts S, Nishiyama T, Hasebe M, Van de**
910 **Peer Y, Rensing SA, Reski R**. **2013**. Reannotation and extended community
911 resources for the genome of the non-seed plant *Physcomitrella patens* provide
912 insights into the evolution of plant gene structures and functions. *BMC Genomics* **14**:
913 498.

26

914 **Figures Legends**

915 **Fig. 1: Phenotype of *Physcomitrella patens* plastid/mitochondrial glutathione**

916 **reductase knock-out lines.**

917 (a). Wildtype (WT), a sensor line with expression of chloroplast-targeted Grx1-

918 roGFP2 (cpGrx1roGFP2 #40) and two independent Δ*gr1* knock-out lines (Δ*gr1* #48,

919 Δ*gr1* #88) after 40 d of growth on agar plates. Bars, 1 mm.

920 (b) Gametophores carrying ripe sporophytes (upper panel) and spore germination

921 after 8 d and 36 d (inlays Δ*gr1*). Bars,1 mm (upper panels), 0.1 mm (lower panels).

922

923
924

27
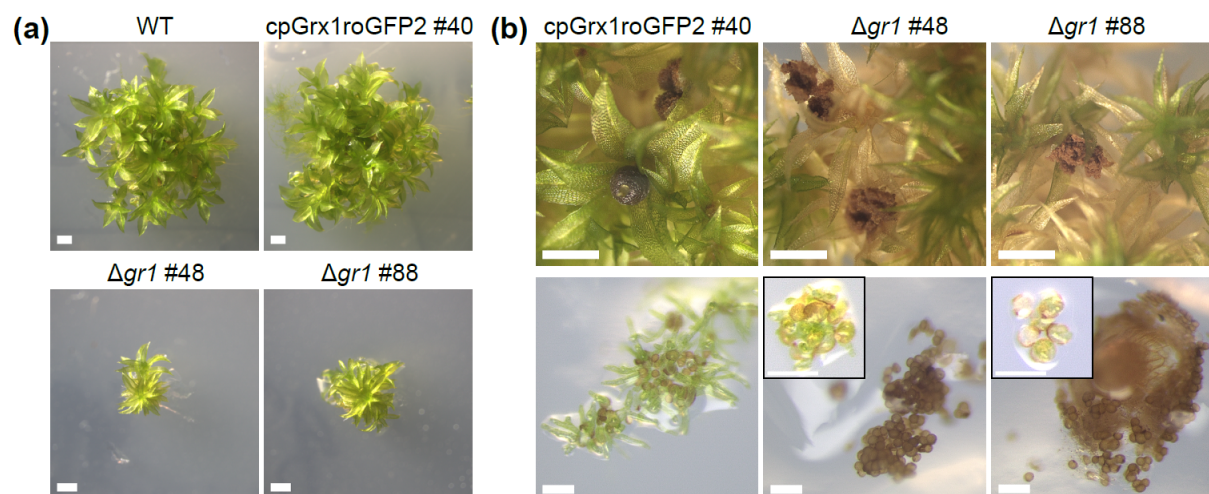
925 **Fig. 2: Chloroplast redox homeostasis in Δ*gr1* plants measured by Grx1-**

926 **roGFP2.**

927 (a) The redox-state of chloroplast-targeted Grx1-roGFP2 was measured

928 ratiometrically by excitation at 405 nm (upper panel, red), and 488 nm (middle panel,

929 green). The emission ratio (lower panel) indicates a highly reduced roGFP2 in WT

930 plastids whereas roGFP2 is nearly fully oxidised in Δ*gr1* lines. Bars, 20 μm.

931 (b) 405/488 nm ratio of plastid Grx1-roGFP2 (*n*=10-30); plot depicts mean +/- SD as

932 boxes, individual data points, and data point density. *** significant difference,

933 *P*<0.001 (one-way ANOVA, TukeyHSD post hoc test). *In vivo* sensor calibration: Red

934 line: 405/488 nm ratio of fully oxidised Grx1-roGFP2 (5 mM 2,2'-dipyridyldisulfide

935 (DPS)); blue line: 405/488 nm ratio of fully reduced Grx1-roGFP2 (10 mM

936 dithiothreitol (DTT)).

937 (c) WT and Δ*gr1* mutant were pre-treated with 2 mM DTT to achieve Grx1-roGFP2

938 reduction and then exposed to continuous laser scanning in water (1 scan/timepoint;

939 WT background *n*=4, Δ*gr1* *n*=9).

940 (d) *In vivo* measurement of light-dependent chloroplast E_{GSH} dynamics. Dark-adapted

941 WT (cpGrx1roGFP2 #40) and Δ*gr1* plants were exposed to a dark/light/dark

942 transition (100 μmol photons m^{-2} s^{-1} for 10 min). Incubation with the electron transport

943 inhibitor 10 μM DCMU blocked the observed E_{GSH} dynamics; *n*=3.


944
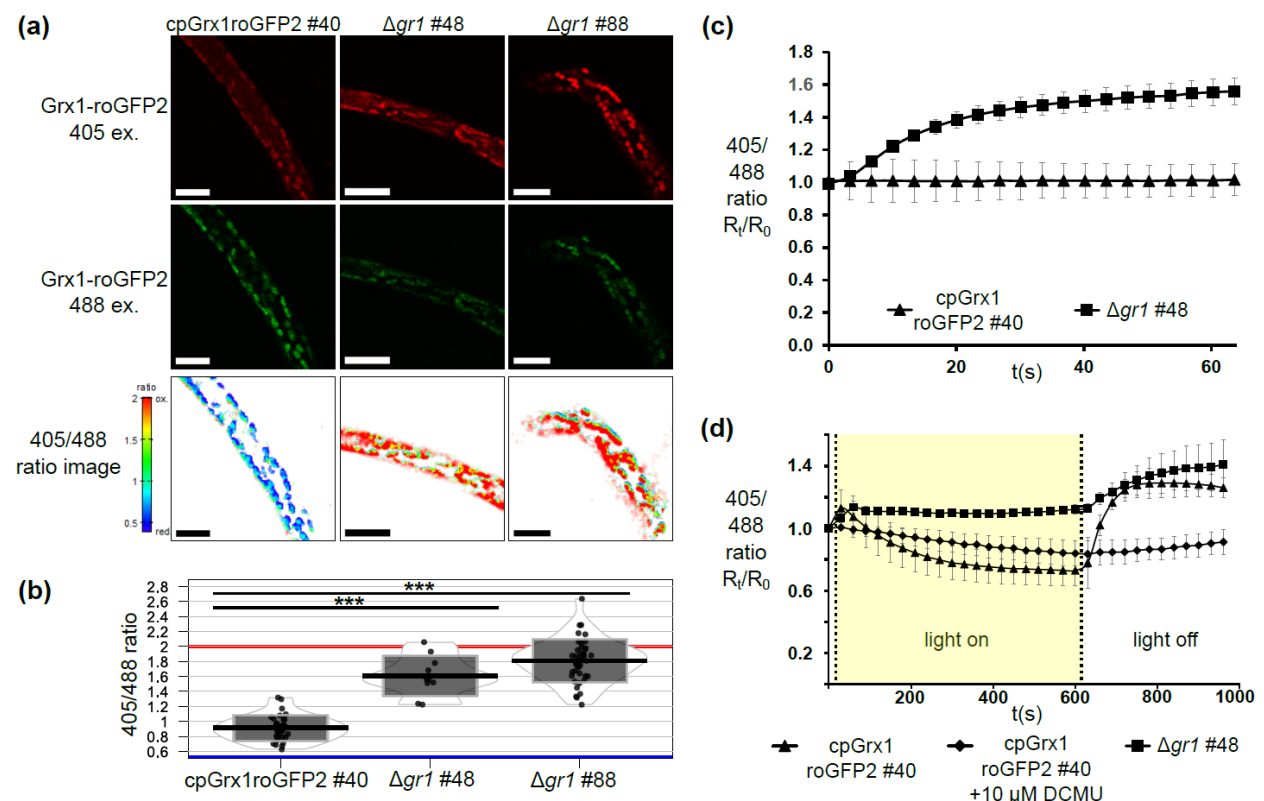
945 **Fig. 3: Ascorbate levels and resistance reactive oxygen species**

946 (a) Total ascorbate (AsA) content of a WT line with the Grx1-roGFP2 sensor and two

947 Δ$gr1$ lines under different light conditions. Lower case letters indicate significant

948 differences ($P<0.05$, two-way ANOVA, Tukey HSD post hoc test).

949 (b) Relative contents of dehydroascorbate and reduced ascorbate in WT and Δ$gr1$

950 plants under different light conditions.

951 (c) Nitro blue tetrazolium (NBT) staining of moss gametophores either kept for 1.5 h

952 in the dark (D) or in the light (120 µmol photons m^{-2} s^{-1}, L). Bars, 100 µm.

953 (d) Plant growth in the presence of Paraquat (upper panel). Survival after transfer to

954 photoheterotrophic growth conditions in the presence of DCMU (3-(3,4-

955 dichlorophenyl)-1,1-dimethylurea) (middle panel) and control of lethal effect of DCMU

956 under photoautotrophic conditions (lower panel). Representative images (n=6-9)

957 shown. Bars, 1 mm.

958

959

960

29
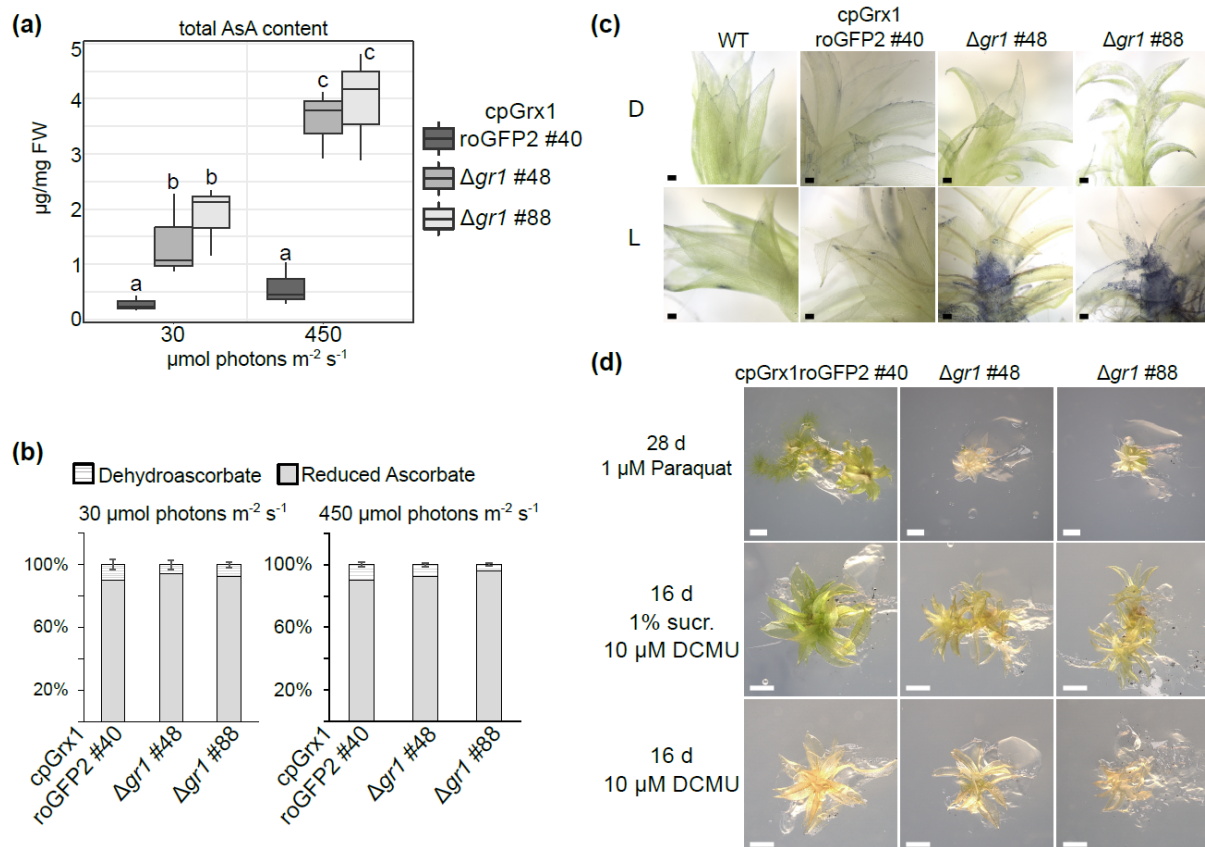
**Fig. 4: Light-sensitivity of Δ*gr1* plants**

(a) High light treatment of plants grown on agar plates (HL, upper panel); bars, 0.5 mm. High light combined with elevated temperature (middle panel), and elevated temperature in the dark (lower panel). Bars, 1 mm.

(b) Photosynthetic parameters measured under low light (LL, 15 µmol photons m^{-2} s^{-1}), control light (C, 50 µmol photons m^{-2} s^{-1}) and high light (HL, 450 µmol photons m^{-2} s^{-1}). Non-photochemical quenching (NPQ, left panel). Bars indicate standard deviation (SD, n=6); white and black boxes on top indicates light and dark phase of the measurements. Actinic light (1076 µmol photons $m^{-2} \cdot s^{-1}$) was switched off after 5 min illumination. Photosynthetic linear and cyclic electron flow (LEF+CEF; middle panel; n=6 LL, CL; n=12 HL). PSI/PSII ratio (right panel; n=6 LL, CL; n=12 HL).

(c) Measurement of the proton motive force components pH gradient and proton conductivity of the ATP synthase (n=3). Left: Dark relaxation of the carotenoid electrochromic shift signal (ECS) after illumination (white box) with 300 µmol photons $m^{-2} \cdot s^{-1}$ (P<0.0001, paired t-test). White and black box on top indicates light and dark phases of the measurements. Membrane potential ΔΨ. Right: Proton conductivity of the ATP synthase g_H^+.

(d) HPLC measurements of zeaxanthin levels in plants grown under low light (LL, 15 µmol photons m^{-2} s^{-1}) and plants grown under control light (C, 50 µmol photons m^{-2} s^{-1}) and shifted for 4 h to high light (HL, 450 µmol photons m^{-2} s^{-1}). n=6, small letters depict significant differences, P<0.05 (two-way ANOVA, Tukey HSD post hoc test), plot depicts mean +/- SD as boxes, individual data points, and data point density.

(e) HPLC measurements of total glutathione level (GSH+GSSG). No significant differences (one-way ANOVA, Tukey HSD post hoc test).

31
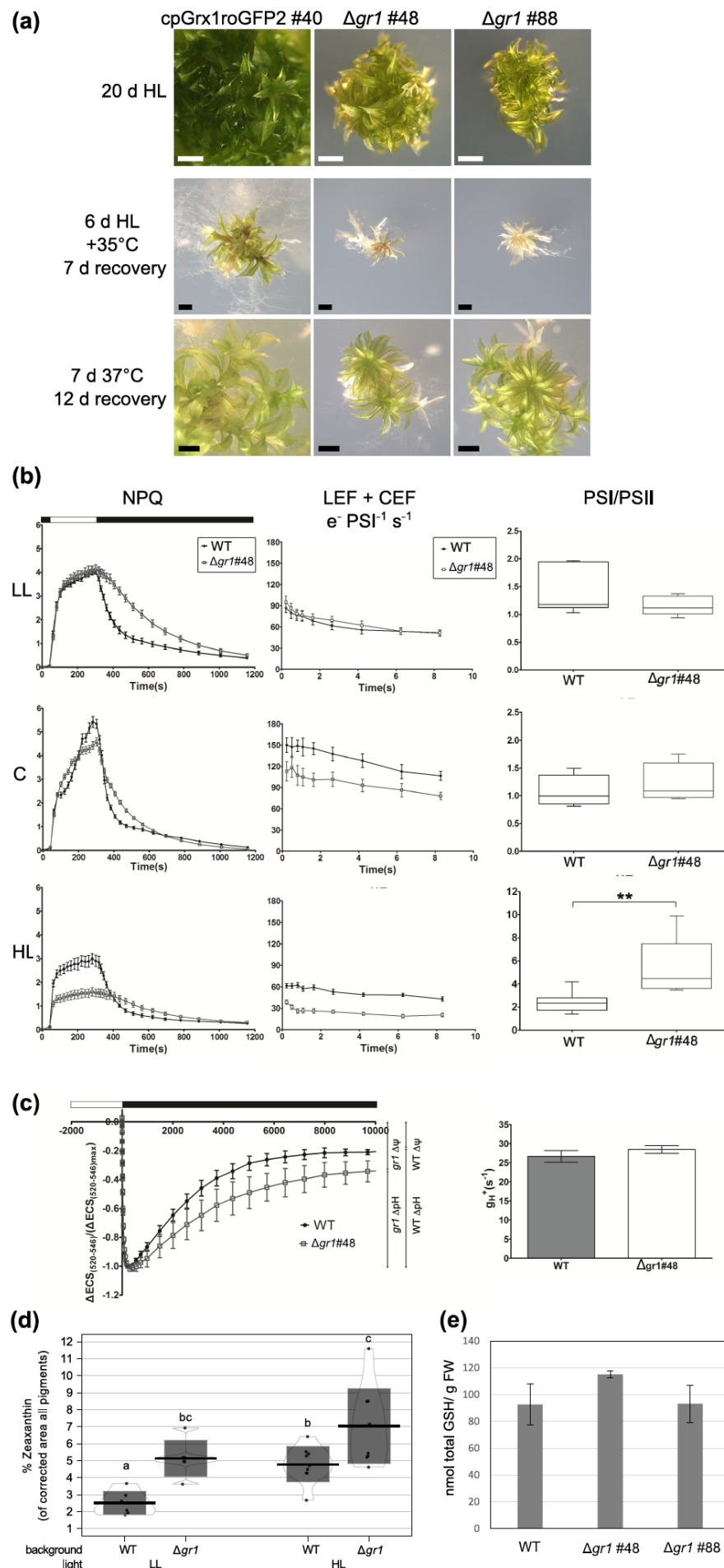
987 **Fig. 5: Quantification of protein abundances by metabolic labelling.**

988 (a) Protein abundances of Δ*gr1*/WT in low light (LL) and after a shift to high light (HL)

989 for 1 h.

990 (b) Area-proportional Venn diagram (Hulsen *et al.*, 2008) showing overlap of proteins

991 with differential abundance (Δ*gr1*/WT) between light treatments.

992 (c) Comparison of manually annotated subcellular localisations (Table S2) of proteins

993 with differential abundance.

994 (d) Cleveland dot plot showing functional categories (Table S2) containing >2

995 proteins with differential abundance (Δ*gr1*/WT). LL, low light; HL, high light; LL+HL,

996 differentially abundant in low light and high light.

997

998

999

32
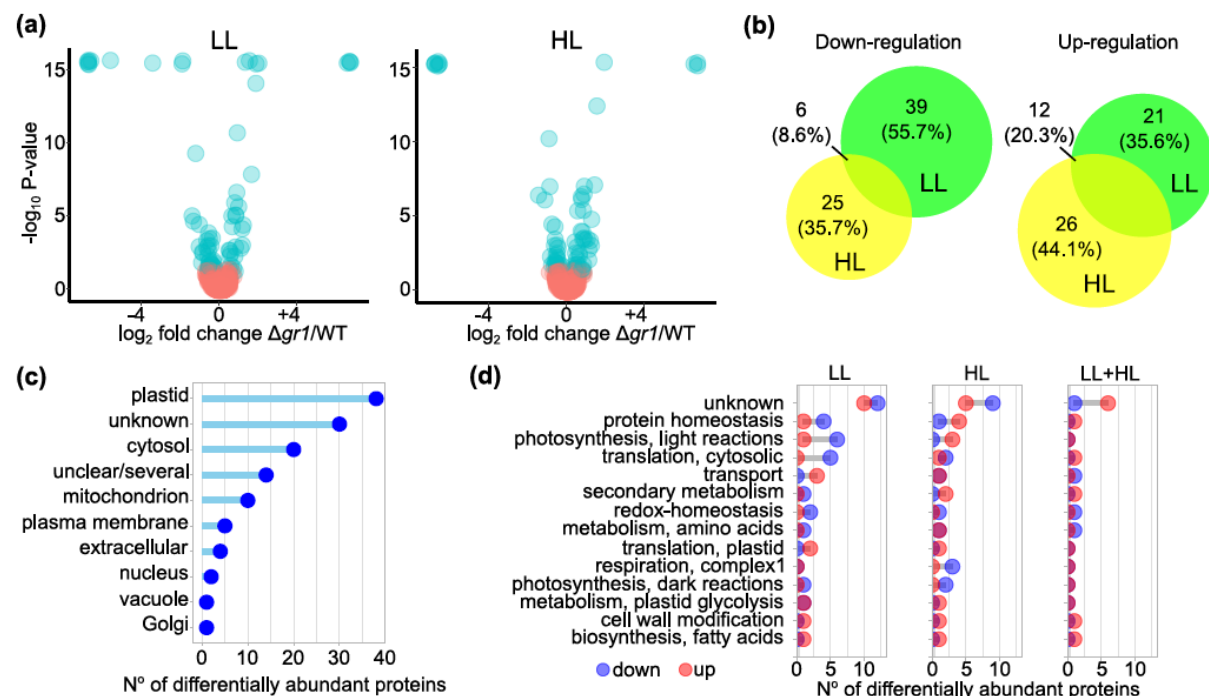
1000 **The following Supporting Information is available for this article:**

1001 Fig. S1 Identification of PpGR1 knock-out mutants.

1002 Fig. S2 Δ*gr1* mutant phenotype details.

1003 Fig. S3 The ultrastructure of chloroplasts is not disrupted in Δ*gr1* mutants.

1004 Fig. S4 Δ*gr1* plants are viable in extended periods of darkness.

1005 Fig. S5 Δ*gr1* plants cannot profit from higher light fluencies.

1006 Fig. S6 Δ*gr1* plants are light-sensitive - measurements of CEF and Fv/Fm.

1007 Fig. S7 Experimental setup for protein quantification via metabolic labelling.

1008 Fig. S8 Verification of GR1 absence in Δ*gr1* by targeted LC-MS/MS.

1009

1010 Table S1 Primer list.

1011 Table S2 Proteomics data and functional annotation (separate file).

33